Conductive and dielectric defects, and anisotropic and isotropic turbulence in liquid crystals: Electric power fluctuation measurements

Tibor Tóth-Katona* and James T. Gleeson
Department of Physics, Kent State University, P.O. Box 5190, Kent, Ohio 44242, USA
(Received 29 April 2003; published 15 January 2004)

Fluctuations of the injected electric power during electroconvection (EHC) of liquid crystals are reported in both the conductive and the dielectric regime of convection. The amplitude and the frequency of the fluctuations, as well as the probability density functions have been compared in these two regimes and substantial differences have been found both in defect turbulence of EHC and at the DSM1→DSM2 transition.

DOI: 10.1103/PhysRevE.69.016302 PACS number(s): 47.65.+a, 61.30.−v, 47.52.+j, 05.40.−a

I. INTRODUCTION

Fluctuations in dissipative systems driven out of equilibrium have attracted considerable attention recently. Examples include universality [1–3], velocity and temperature spectra [4], correlations [5–8], and the fluctuation probability density function (PDF) [9–13]. These works have focused mainly on the following: (i) understanding fluctuations within the framework of phase transitions in equilibrium systems, (ii) finding a universal form of the fluctuations in different systems, (iii) investigating why fluctuations often obey non-Gaussian PDF's, and (iv) investigating the origin of the low-frequency oscillations of large-scale flows observed in Rayleigh-Bénard convection. It is important to note here that all the listed experimental/numerical results have been obtained for flow of *isotropic* fluids.

In parallel to the above-mentioned works, another method has been demonstrated in Refs. [14,15] to study electrohydrodynamic convection (EHC) in liquid crystals, based on detection of a global quantity, namely, the injected electric power P. Note that the mean value of the injected power $\langle P \rangle$ has to be the same as the mean value of the dissipated power. However, the fluctuations around these mean values do not need to be the same [11]. This method opens new routes in investigations of fluctuations in a well-studied, driven, dissipative system. EHC lends itself quite naturally to the study of such fluctuations, because the basic fluid instability is driven by sustaining an electric potential difference, and so it is straightforward to characterize both the injected power and the fluctuations therein by measuring the electric current. Furthermore, EHC in nematic liquid crystals has numerous advantages for these types of studies over other driven fluid flow systems: there are rich varieties of convective states (see, e.g., Ref. [16]), employing a large aspect ratio (which minimizes lateral boundary effects) is much simpler in EHC than for Rayleigh-Bénard convection and the relevant control parameter(s) (the driving voltage U and the temperature T) are easily and precisely tunable. One important feature of EHC not found in the systems listed above is their inherent *anisotropy*. Anisotropy permits the Carr-Helfrich instability by which an electric potential difference can cause flow. The anisotropic nature of nematic liquid crystals means their flow is not described by the Navier-Stokes equation, but by the Ericksen-Leslie equations, in which the orientational degrees of freedom are coupled to the flow field [17]. Lastly, EHC exhibits a particularly rare phenomenon: an abrupt turbulence to turbulence transition [18], as opposed to other fluid flow systems in which one observes different regimes of turbulence, but there are no well-defined thresholds for the onset of these regimes.

The aim of this paper is to compare injected power fluctuations in two distinct states, namely, the conductive and the dielectric regimes of electroconvection. We focus on both the defect turbulence regime (in which the spontaneous generation/annihilation of dislocations destroys the stationary EHC roll pattern by breaking the rolls into moving segments) and on the transition from anisotropic to isotropic turbulence (the DSM1-DSM2 transition).

Considerable differences have been found between the defect turbulence state in conductive and dielectric regimes of EHC. In the conductive regime [19] spatial coherence is absent, however, a dominant length scale still survives [20]. More recent experiments in conductive regime defect turbulence show that despite the spatial incoherence, temporal correlations persist over extremely long time due to global, quasiperiodic oscillations in the injected electrical power; these oscillations are associated with the defect creation/annihilation rate [21]. On the other hand, the dielectric regime defect turbulence has quite different characteristics as pointed out in Ref. [22]. In a narrow voltage range above the onset of defect turbulence, defects (with topological charge ± 1) are generated/annihilated in pairs without spatial correlation; the number of these defects increases with voltage. Slightly above the onset of defect turbulence, at a fairly well-defined threshold, defects start to develop spatial correlation; they form chains (parallel to the original roll direction) of the same topological charge alternating in space leading to the chevron pattern. Concomitantly, with the restitution of the spatial correlation a significant increase in the density of defects has been observed. With further increase of the voltage collective defect motion occurs [22]. One natural question is how such a spatiotemporal order will influence the fluctuations in a global quantity like P, especially knowing that

*On leave from Research Institute for Solid State Physics and Optics, Hungarian Academy of Sciences, H-1525 Budapest, P.O.B. 49, Hungary.

 ©2004 The American Physical Society

spatially incoherent defect creation/annihilation in conductive defect turbulence leads to a persistent temporal correlation [21].

Another motivation of the present work is the observation that the transition from anisotropic to isotropic turbulence [18] has no apparent signature in electric Nusselt number [14,15]. This is surprising in the light of previous studies on the DSM1→DSM2 transition in the conductive regime that have shown that above a critical voltage U_t, DSM2 state replaces the DSM1 state by nucleation and growth, via passage of a distinct front separating the two states [18,23–31]. The transition is characterized by an abrupt increase in the density of disclination loops [23,24,26,27], and the transition voltage depends on the ramp rate r [23,24,29], on the sample thickness [31], on the anchoring strength [28,30,31], and on the driving frequency [25,30].

II. EXPERIMENTAL SETUP

For the measurements a similar experimental setup has been used as described in Ref. [15]. The sinusoidal voltage signal is generated using the internal function generator of a lock-in amplifier. This signal is amplified and applied across the liquid crystal (LC) layer sandwiched between two glass plates. The current traversing through the LC sample is fed into the field-effect transistor input of a current-to-voltage preamplifier. The output of this preamplifier is measured by the lock in. The lock in time constant is set to just above the period of the signal frequency. The in-phase output of the lock in is amplified to bring the signal into the optimal range for an analog-digital computer whose output is recorded by a personal computer. For each experimental point an optical image taken through a polarizing microscope using the shadow-graph technique has been also recorded. This recording is especially useful if one takes into account the temporal changes in the electric properties of liquid crystals (see later discussion). The experimental setup proposed by Ref. [32] (with a voltage divider instead of current-to-voltage preamplifier) has been also tested and no significant differences have been found between the results obtained by the two methods.

We used the liquid crystal mixture Mischung V (M5) with 2.73 wt% dopant (as proposed in Ref. [33]). This material possesses good chemical stability, a relatively broad nematic range, and known material parameters [33]. Moreover, the electrical conductivities change sufficiently with temperature allowing us to conduct measurements at constant frequency (see below). Most of the measurements presented below have been carried out at $T=(25.00\pm0.01)$ ° C and at $T=(50.00\pm0.01)$ ° C, where a satisfactory spatial homogeneity of the samples is ensured (see later discussion).

The sandwich cells have been prepared with etched electrodes of area $A=1$ cm^2 (cell A), $A=0.5$ cm^2 (cell B), and $A=0.0615$ cm^2 (cell C—the sample on which most of the experiments presented here are performed) with thickness $d=(16.7\pm0.3)$ μm, $d=(51\pm1)$ μm, and $d=(33.4\pm0.2)$ μm, respectively, providing aspect ratios of $s=\sqrt{A}/d\approx600$, 136, and 74.

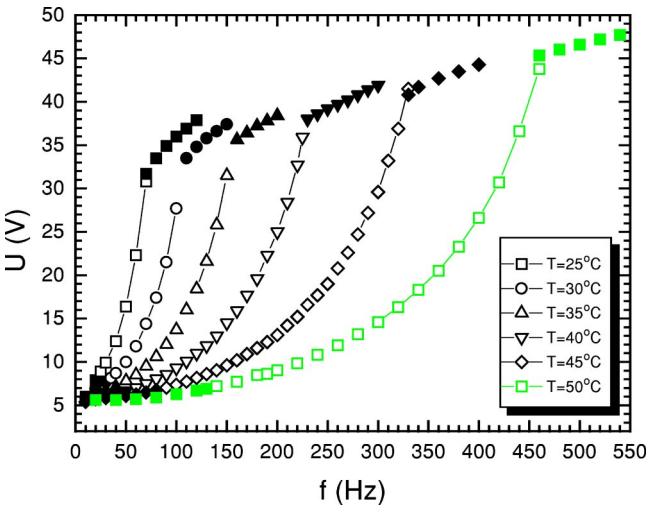

FIG. 1. (Color online) Phase diagram of EHC at different temperatures T. The closed symbols in the low-frequency range denote stationary (normal or oblique) rolls. Open symbols stand for the nonstationary, traveling rolls and in the high-frequency range the closed symbols are for dielectric normal rolls.

III. EXPERIMENT

A. Phase diagram

The phase diagram of EHC is shown in Fig. 1 for different temperatures T measured in cell A. The closed symbols at low frequencies f denote the threshold of a stationary conductive roll pattern of EHC (normal rolls—NR or oblique rolls—OR) as the first bifurcation, while nonstationary traveling rolls are marked with open symbols. The closed symbols in the high-f range stand for the dielectric normal rolls. The choice of the working frequency for the fluctuation measurements is restricted with the spatial inhomogeneity of the sample. Namely, the recorded signal is integrated over the active area of the sample (where the electrodes overlap) and consequently, it is required that at a given voltage U the same EHC pattern appear in the whole cell. At frequencies where $U(f)$ becomes steeper the EHC pattern gets less homogeneous in space. For example, at $T=50$ °C above $f=250$ Hz the threshold U_c of EHC differs by $\Delta U\approx1$ V at different locations of the cell. Therefore, for further measurements $f=100$ Hz has been chosen, where ΔU was found less than 0.02 V at $T=50$°C and where for the dielectric regime of EHC at $T=25$ °C ΔU was undetectable.

On the other hand, Fig. 1 explains the difficulties to perform precise measurements on the electric properties of the nonstationary, traveling rolls of EHC (open symbols): at all temperatures where the Hopf bifurcation (open symbols in Fig. 1) is observed, $U(f)$ gets steep and the spatial inhomogeneity of the EHC pattern cannot be neglected.

B. Conductivity

Before performing the power fluctuation measurements, the conductivity G of the sample has been determined as a function of the applied voltage. The applied voltage has been increased in small steps (≈0.1 V with a waiting time of 30 s between each step), similar to the measurements presented in

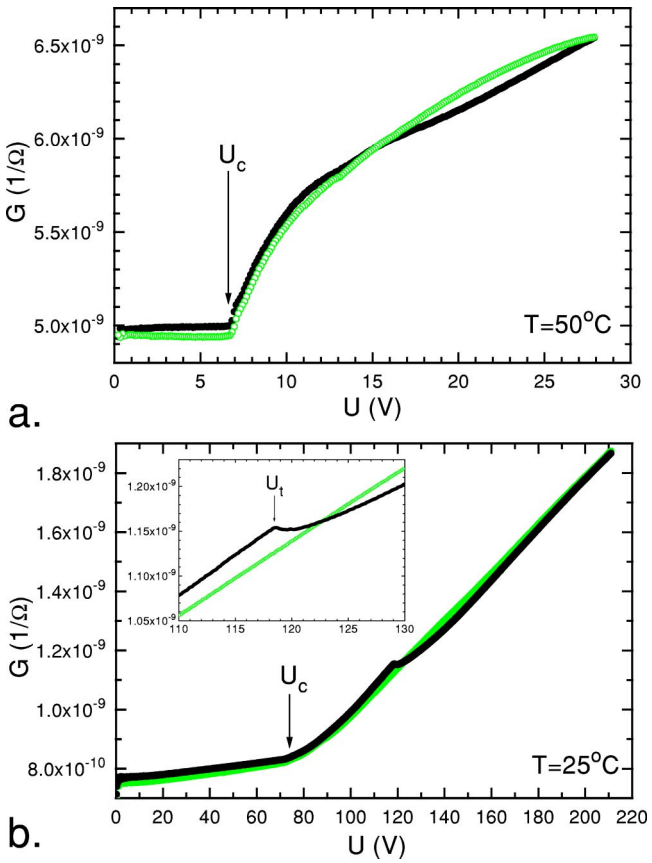

FIG. 2. (Color online) Conductivity G vs the applied voltage U in a cycle with increased voltage steps (black, closed symbols) followed by decreased voltage steps (light, open symbols) at (a) $T=50\,^{\circ}\mathrm{C}$ (conductive regime of EHC) and at (b) $T=25\,^{\circ}\mathrm{C}$ (dielectric regime). The inset shows blowup of the voltage range where the anisotropic-isotropic turbulence transition takes place.

Ref. [34]. Also, a snapshot of the pattern has been recorded for each point just before reading out the electric current. The results are shown in Fig. 2 for cell C with increased voltage steps (black, closed symbols) followed immediately by decreasing voltage steps (open symbols) at two temperatures $T=50\,^{\circ}\mathrm{C}$ (conductive EHC) and $T=25\,^{\circ}\mathrm{C}$ (dielectric EHC).

At $T=50\,^{\circ}\mathrm{C}$ both sets (increased and decreased steps in U) of measurements clearly show the onset of EHC at $U_c=6.97$ V which are in excellent agreement with the optical observations presented in Fig. 3(a) which place the onset of EHC at $U_c=(6.97\pm0.05)$ V with oblique rolls (OR) as the first bifurcation.

At $T=25\,^{\circ}\mathrm{C}$, U_c is found to be (73.3 ± 0.1) V from the $G(U)$ curves [Fig. 2(b)]; which is again in agreement with the onset of the dielectric normal rolls (NR) obtained by shadowgraph technique [Fig. 3(b)] at $U_c=(73.2\pm0.5)$ V. Note the virtual mismatch of U_c between Figs. 1 and 2(b). However, the data in these two figures have been obtained for different samples having thickness d differing by a factor greater than 2. The thicker sample [cell C, Fig. 2(b)] must have higher cutoff frequency f_c (separating the voltage dependent conductive regime of EHC from the electric field dependent dielectric regime) than the thinner sample (cell A,

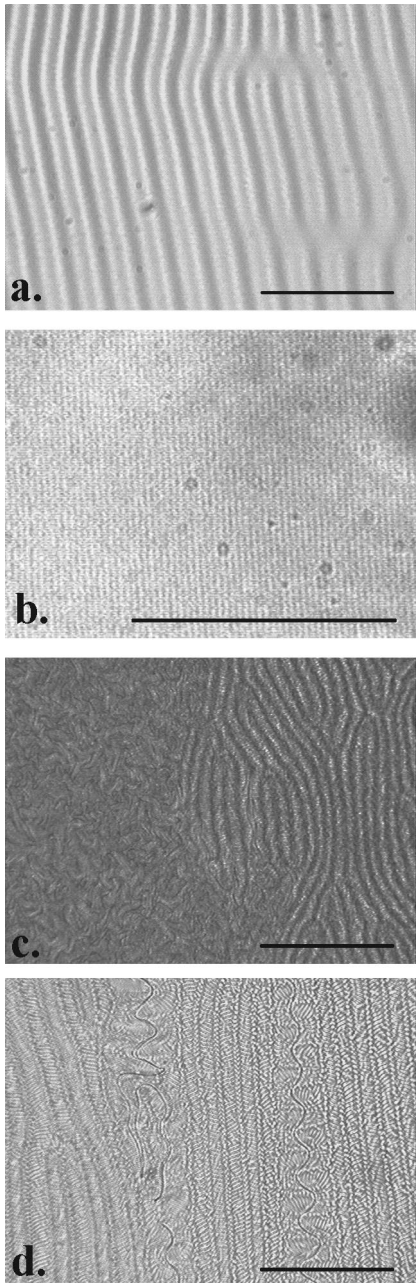

FIG. 3. Snapshots of the EHC patterns at characteristic points shown in Fig. 2. (a) at $T=50\,^{\circ}\mathrm{C}$ and at the threshold $U_c=6.97$ V of the oblique rolls; (b) at $T=25\,^{\circ}\mathrm{C}$ and at the threshold $U_c=73.2$ V of the dielectric normal rolls; (c) at $T=25\,^{\circ}\mathrm{C}$ and at the anisotropic-isotropic turbulence transition voltage $U_t=118.5$ V showing the transition front passing through the sample; (d) a demonstration of persistence of the disclination loops in the case of decreased voltage steps at $T=25\,^{\circ}\mathrm{C}$ and $U=88.2$ V. The scale bars show 100 μm.

Fig. 1). Taking this into account it is easy to understand the difference (by a factor of about 2) in U_c between Figs. 1 and 2(b).

Figure 2 also shows an important feature common to all liquid crystals investigated by us (MBBA, phase 5, M5). For all these materials, the conductivity decreases slightly if they are exposed to a considerable voltage for longer time ($\sim$

hour). This behavior is the best seen at $U<U_c$ where the values of G measured with decreased U steps are considerably lower than those previously recorded with increased U steps. One has to note also that at $T=50\,^{\circ}\mathrm{C}$ below U_c our sample behaves as an Ohmic resistor (G independent of U), while at $T=25\,^{\circ}\mathrm{C}$ its electric properties seem to be non-Ohmic.

Above U_c, $G(U)$ appears to be more complicated. For both temperatures $T=50\,^{\circ}\mathrm{C}$ and $T=25\,^{\circ}\mathrm{C}$ a crossover occurs in $G(U)$ between the data recorded with increased voltage steps and those with decreased voltage steps. For the conductive EHC [Fig. 2(a)] this crossover has been found close to U (but not at the exact value) where long-time oscillations in the autocorrelation function $g_a(t)$ diminish (see the following section). For dielectric EHC [Fig. 2(b)], however, the crossover takes place just above the anisotropic-isotropic turbulence transition voltage U_t [see inset of Fig. 2(b)]. Namely, in the measurements with increased voltage steps a local maximum of $G(U)$ has been detected at $U_t=118.5$ V exactly at the voltage where the front from anisotropic to isotropic turbulence transition (DSM1-DSM2 [18]) has been optically observed [Fig. 3(c)]. This transition is characterized by formation of disclination loops that become detectable if one abruptly zeros U [26]. The absence of this local maxima in the case of the decreasing voltage steps can be understood considering Fig. 3(d): disclination loops persist down up to a voltage $U\approx 88$ V under our experimental conditions (voltage steps of ≈ 0.1 V and waiting time of 30 s between each step) showing an extremely large hysteresis [35].

C. Electric fluctuations

Measurements on the current/power fluctuations have been performed as follows. The time constant of the lock-in amplifier has been set to 30 ms (as usually in the other measurements) and the sampling time of about 50 ms has been chosen for all the fluctuation measurements. For each driving voltage U, 65 536 experimental points have been recorded (i.e., about a 1 h run for each data set). All sets of measurements have been carried out with increasing voltage steps and with a waiting time of about 20 min after increasing U (and before starting the fluctuation measurements) to achieve a stationary state of EHC. Snapshots of the EHC patterns have been recorded immediately before starting and after finishing the experimental run (in contrast to the conductivity measurements, here we were unable to record an optical image for each experimental point since it would drastically increase the sampling time).

Figure 4 shows the standard deviation of the power fluctuations σ_P normalized with the mean value of the power $\langle P\rangle$ as a function of the dimensionless driving voltage $\varepsilon=(U/U_c)^2-1$ in cell C. The open symbols denote measurements performed at $T=50\,^{\circ}\mathrm{C}$ (conductive OR at $\varepsilon=0$), while closed symbols stand for measurements at $T=25\,^{\circ}\mathrm{C}$ (dielectric NR at $\varepsilon=0$).

A dramatic increase of $\sigma_P/\langle P\rangle$ slightly above $\varepsilon=0$ in conductive EHC has been detected recently [32] and has been assigned to the creation/annihilation of defects [21]

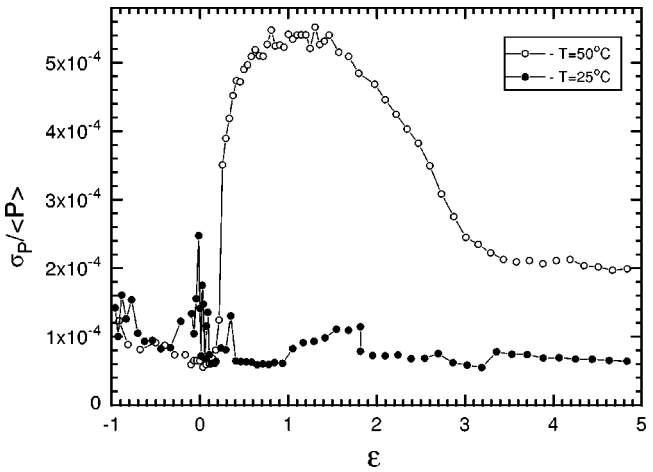

FIG. 4. The standard deviation of the power fluctuations normalized with the mean value of electric power $\langle P\rangle$ as a function of the dimensionless driving voltage ε in the conductive regime of EHC (open symbols) and in the dielectric regime of EHC (closed symbols).

starting at $\varepsilon\equiv\varepsilon_d\approx 0.2$. As it has been shown in Ref. [21] for cells A, B, and C, the increase of $\sigma_P/\langle P\rangle$ strongly depends on the aspect ratio s of the sample: for smaller s, there is a larger increase in $\sigma_P/\langle P\rangle$. This is one of the reasons why we discuss cell C (with the smallest s among our samples) in the rest of the paper. In this sample an increase of $\sigma_P/\langle P\rangle$ by about an order of magnitude occurs at the threshold $\varepsilon_d\approx 0.2$ of the defect creation/annihilation.

In dielectric regime of convection the defect creation/annihilation process starts at somewhat lower threshold $\varepsilon_d\approx 0.03$ and in contrast to the conductive EHC, here no significant increase of $\sigma_P/\langle P\rangle$ has been found at and above ε_d as one can see from Fig. 4. The amplitude of the power fluctuations at $\varepsilon\ll 0$ has been found to be comparable in both conductive and dielectric EHC. For dielectric convection at $\varepsilon<0$ (above $\varepsilon\approx -0.3$) where the EHC pattern is not yet formed, a slow motion of small dust particles has been detected indicating the presence of some kind of flow. In this voltage range power fluctuations show relatively expressed intermittentlike character (sharp changes with relatively large amplitude in P) which fades out above $\varepsilon\approx 0.07$, however, does not disappear completely with further increase of ε (see the later discussion about the probability density function). The fact that the motion of dust particles and the intermittentlike fluctuations appear at the same voltage leads us to a conclusion that the intermittent behavior is presumably caused by a large-scale flow. We mention here that at similar (relatively high) voltages a flow (even in the isotropic phase) has been reported for highly doped MBBA below $\varepsilon=0$ and is considered as a potential cause of formation of the so-called prewavy pattern appearing close to, but still below $\varepsilon=0$ [36]. In samples with highly doped M5 (not discussed here) we observed the same prewavy pattern as it has been described in MBBA and in phase 5 previously [36,37]. This intermittentlike character of the fluctuations in the range of $-0.33\leqslant\varepsilon\leqslant 0.1$ causes a slight increase (by a factor of about 2) of $\sigma_P/\langle P\rangle$. However, this increase is much smaller than

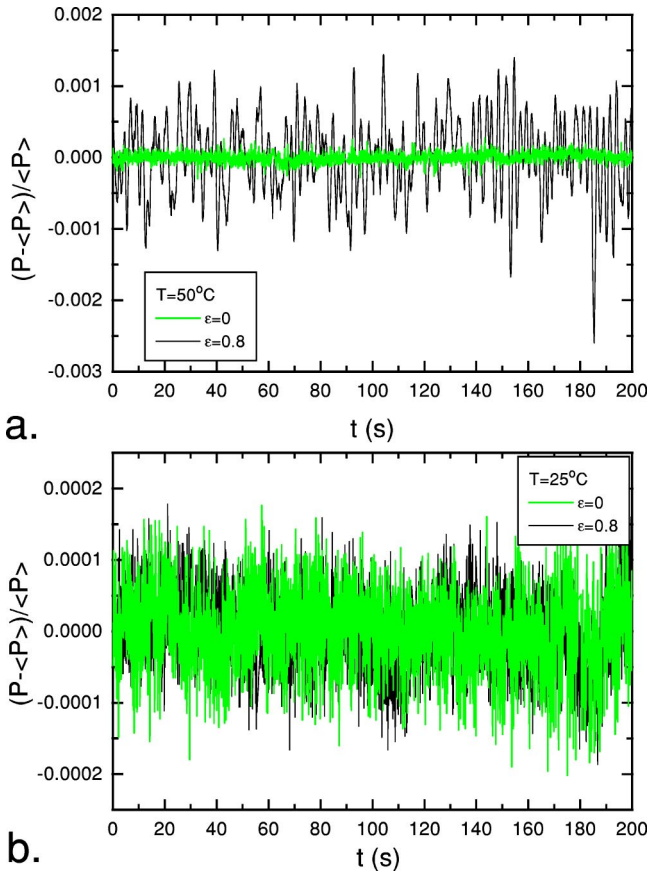

FIG. 5. (Color online) Electric power fluctuations at same values of voltage ε in the conductive (a) and dielectric regime of EHC (b).

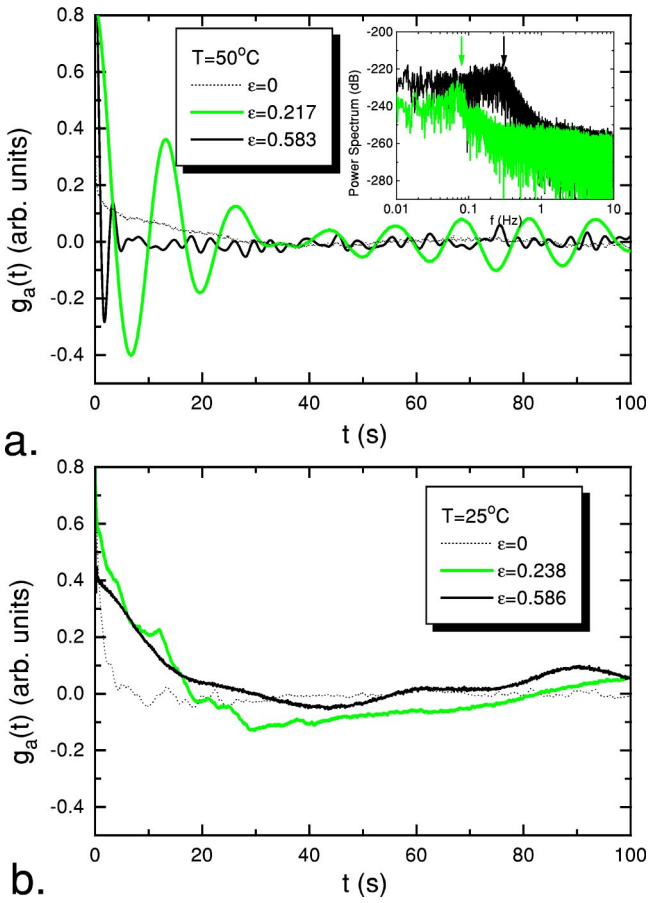

FIG. 6. (Color online) Autocorrelation functions $g_a(t)$ at similar values of ε in the conductive- (a) and in the dielectric regime of EHC (b). Inset in (a): power spectra of fluctuations demonstrating quasiperiodicity at $\varepsilon=0.217$ and at $\varepsilon=0.583$.

that in the conductive EHC and definitely cannot be connected to the creation/annihilation of defects.

With further increase of voltage, at $\varepsilon\approx 0.35$ where the dielectric chevron pattern (see e.g., Ref. [22]) is formed, $\sigma_P/\langle P\rangle$ decreases and stays constant (see Fig. 4) over a considerable range of ε in which defect chains stay aligned parallel to the original roll direction [22]. At $\varepsilon\approx 1$ another transition occurs; the defect chains are no longer aligned parallel to the original roll direction but are deformed as demonstrated in the right-hand side of Fig. 3(c). We consider this pattern as dielectric DSM1, because with further increase of ε the next transition is identified as a transition to DSM2 [see Fig. 3(c)]. At the transition point from dielectric chevron to DSM1 a small, but systematic increase in $\sigma_P/\langle P\rangle$ has been detected (Fig. 4). This monotonic increase in $\sigma_P/\langle P\rangle$ is observable up to the DSM1$\rightarrow$DSM2 at $\varepsilon\approx 1.7$ [Fig. 3(c)] where a small but abrupt decrease in $\sigma_P/\langle P\rangle$ has occurred (Fig. 4).

Another difference between fluctuations in conductive and dielectric EHC is displayed in Fig. 5. Figures 5(a) and 5(b) show power fluctuations at the onset of EHC ($\varepsilon=0$) and at $\varepsilon=0.8$ (black lines) where so-called defect turbulence [38] takes place in the conductive, and in the dielectric EHC, respectively. Figure 5(a) shows a large increase in the fluctuation amplitude (already seen in Fig. 4 and studied in details in Refs. [32,21]). This demonstrates another feature of the fluctuations in conductive EHC. Above ε_d the large amplitude fluctuations become quasiperiodic with a dominant frequency f^* that increases with increase of ε (and depends also on d [21]), but remains much smaller than the driving frequency. For example, for cell C represented in Fig. 5(a), values of f^* have been found in the range between 0.08 Hz (at $\varepsilon_d=0.21$) and 3.12 Hz (at $\varepsilon=7.5$—above this value the quasiperiodic oscillations diminish as it has been shown in Ref. [21]). As described in Ref. [21], f^* exactly corresponds to the creation/annihilation rate of defects (determined from independent optical observations). The increase of f^* with the increase of ε follows convincingly the predictions of the Villermaux's model [5] for the Rayleigh-Bénard convection as has also been shown in Ref. [21].

For dielectric EHC [Fig. 5(b)], however, only a slight increase has occurred in the amplitude of the fluctuation due to the increase of the driving voltage ε from 0 to 0.8, without any detectable change in the spectra of fluctuations. Moreover, in dielectric regime $\sigma_P/\langle P\rangle$ at and above $\varepsilon=0$ stays close to the value of $\sigma_P/\langle P\rangle$ measured at $\varepsilon=0$ for conductive EHC (see Fig. 4).

The normalized autocorrelation function of the power fluctuations $g_a(t)=\langle P(t')P(t'+t)\rangle/\langle P\rangle^2-1$ presented in Fig. 6 for conductive [Fig. 6(a)] and for dielectric EHC [Fig.

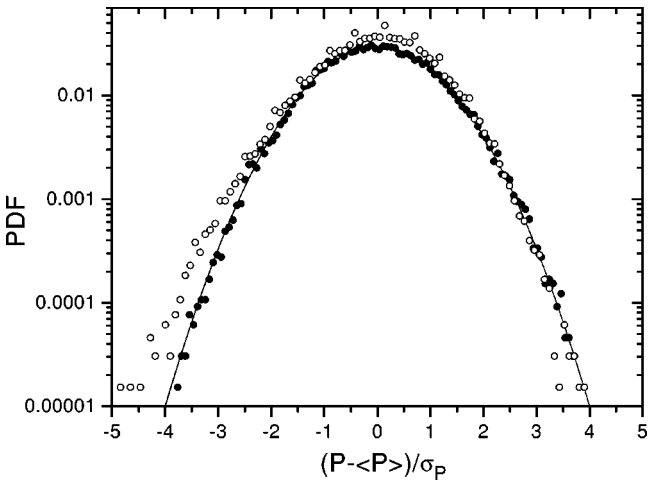

FIG. 7. Probability density function (PDF) of the power fluctuations above the onset of EHC, at $\varepsilon \approx 0.6$ for $T=50\,^{\circ}\mathrm{C}$ (conductive EHC, filled symbols) and for $T=25\,^{\circ}\mathrm{C}$ (dielectric EHC, open symbols). The line shows the Gaussian distribution with no fitting parameters.

6(b)] also shows features described in preceding two paragraphs. For conductive EHC, above ε_d slow, persistent oscillations occur in $g_a(t)$ (see for details Ref. [21]). The oscillation frequency again corresponds to f^* (and to the optically determined creation/annihilation rate of defects) [21]. The inset of Fig. 6(a) shows the power spectra of injected power fluctuations at $\varepsilon=0.217$ and at $\varepsilon=0.583$. Low-frequency peaks in the spectra demonstrate the presence of quasiperiodicity. The arrows indicate the frequencies f^* obtained from independent, optical measurements. In contrast, in dielectric EHC no oscillations have been observed in $g_a(t)$ at similar ε values [see Fig. 6(b)] nor at any investigated ε up to $\varepsilon \approx 5$.

The PDF of the power fluctuations has been also investigated. In cell C, over the whole voltage range in which the defect turbulence state in the conductive regime is present, no systematic deviation from the Gaussian distribution has been found as reported already in Ref. [32] for another liquid crystal material, MBBA. Filled symbols in Fig. 7 show a typical distribution in this defect turbulence voltage range, while the line represents the Gaussian function with no fitting parameters. In dielectric EHC, however, a systematic departure from the Gaussian distribution has been found in the whole voltage range of the defect turbulence. Empty symbols in Fig. 7 show the typical deviation from the normal distribution at about the same $\varepsilon \approx 0.6$ as for the conductive EHC (filled symbols). Obviously the maximum of the PDF is shifted towards $P-\langle P\rangle>0$, the tail of the distribution in the region $P-\langle P\rangle<0$ is systematically shifted towards larger negative values of $P-\langle P\rangle$ than for the Gaussian form, almost showing an exponential dependence. At the same time, on the positive side at the tail data are a bit smaller than those for the normal distribution.

No detectable change in the character of the PDF has been observed at DSM1→DSM2 transition in dielectric EHC—the distribution remains similar to that shown in Fig. 7 (empty symbols). In conductive EHC the situation is more

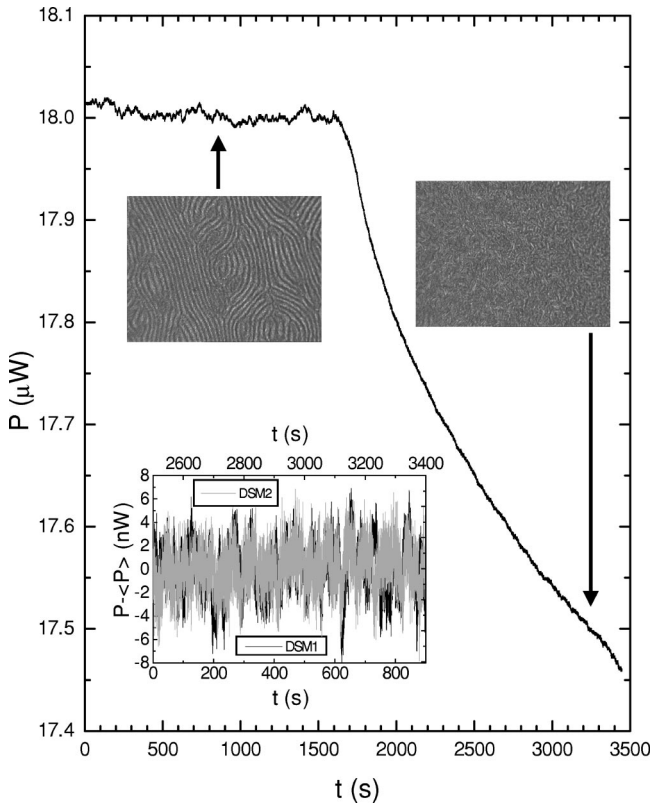

FIG. 8. Electric power measurement at the anisotropic-isotropic turbulence transition in dielectric EHC ($T=25\,^{\circ}\mathrm{C}, \varepsilon_t=1.83$). The insets show the optical patterns as well as power fluctuations in DSM1 (black line, pattern on the left-hand side) and DSM2 (light line) turbulence.

complicated. Namely, the set of our fluctuation measurements show a small, but systematic departure of PDF from the Gaussian distribution above $\varepsilon \approx 40$ (deeply in DSM1 turbulence voltage range) [39]. However, above DSM1 →DSM2 transition, at $\varepsilon_t \approx 60$, the power fluctuations again obey Gaussian statistics, which remains the case up to extremely high values of $\varepsilon > 800$, where a clearly non-Gaussian distribution is obtained [39]. We mention here that optical observations place ε_t in a wide voltage range of $30 < \varepsilon_t < 200$ depending on the experimental conditions (ramp rate, sample thickness, for how long and to which voltage the sample has been exposed, etc.) which is too wide to make a conclusive comment on PDF at the anisotropic-isotropic transition in conductive EHC. Up to the present, it seems that the DSM1→DSM2 transition is not accompanied with a significant change in PDF of power fluctuations, which is difficult to reconcile with the results of Ref. [27] where (for conductive EHC) a distinct change in PDF of ''surrogate of the local distortion energy density'' has been obtained at this transition point.

In the electric power fluctuation measurements the DSM1→DSM2 turbulence transition has been observed at $\varepsilon_t=1.83$ for dielectric EHC (see the snapshots of the patterns in Fig. 8 taken at the beginning and at the end of the fluctuation measurement). If one compares this value of ε_t with that obtained from the conductivity measurements [inset of

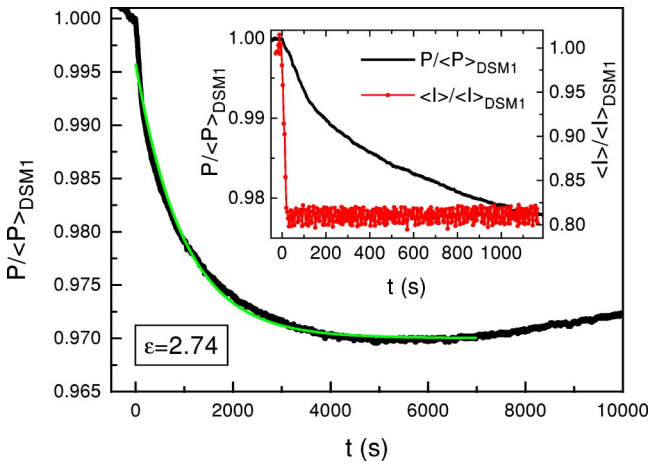

FIG. 9. (Color online) Temporal dependence of the injected power P in DSM2 (dielectric EHC) turbulence normalized with P_{DSM1} measured in DSM1 (thick line). The DSM1-DSM2 transition takes place at $t=0$; $T=25\,^{\circ}\mathrm{C}$; $\varepsilon=2.74(>\varepsilon_t)$. Thin line represents an exponential decay fit to the data. The inset compares temporal dependence of $P/\langle P\rangle_{DSM1}$ with that of the normalized transmitted light intensity $\langle I\rangle/\langle I\rangle_{DSM1}$.

Fig. 2(b), $\varepsilon_t=1.61$] a significant difference is seen between them, which can be explained by the ''electric history'' (for how long and to which voltage the sample has been exposed) of the sample. Namely, because the entire conductivity measurement shown in Fig. 2(b) is performed within 36 h, the sample was therefore exposed to a (different) voltage for about 9 h before ε_t is reached. In fluctuation measurements, however, the sample was exposed to a voltage for about 60 h (while other fluctuation measurements at $\varepsilon<\varepsilon_t$ were performed). Now, it is more clear why did we observe such a broad range of ε_t for the conductive EHC: in some of those threshold measurements we approached ε_t with quick voltage steps while in others we have waited for hours between the steps. The electric history of the sample, however, does not change the cutoff frequency significantly as revealed by control measurements at the beginning and at the end measurements (after several weeks) which demonstrates the high chemical stability of M5 as pointed out in Ref. [33].

The inset of Fig. 8 shows the power fluctuations at ε_t both in isotropic (DSM2, light line) and anisotropic turbulence (DSM1, black line). The spectra of the fluctuations does not seem to differ significantly in these two regimes. However, the width of the fluctuations σ_P is considerably smaller in DSM2 than that in DSM1. The smaller σ_P in DSM2 than in DSM1 (despite of decay in P discussed in the following paragraph) causes a small, but abrupt decrease of $\sigma_P/\langle P\rangle$ at ε_t as shown in Fig. 4.

The main plots of Figs. 8 and 9 show that the injected electric power decays exponentially at the anisotropic-isotropic turbulence transition. The decay time is rather surprising. Namely, the anisotropic-isotropic turbulence transition finishes within few seconds (at some moment isotropically turbulent regions nucleate and invade the whole anisotropic area in the cell within 1 min). However, the decay time of P is much larger than a minute as one sees from Fig. 9: the exponential fit has decay time of $\tau=975$ s, and P saturates after several hours even if $\varepsilon>\varepsilon_t$ as demonstrated in Fig. 9. This figure shows for dielectric EHC the temporal dependence of the injected power P in DSM2 turbulence normalized with the power P_{DSM1} measured in DSM1 at $\varepsilon=2.74(>\varepsilon_t)$. The DSM1$\rightarrow$DSM2 transition takes place at $t=0$. As one can see, even for this relatively high ε, P saturates more than an hour after the DSM1$\rightarrow$DSM2 transition at a value of P lower than P_{DSM1} by about 3%. About 2 h after the transition P starts to increase slowly, however, it is still below the value of P_{DSM1}.

In order to elucidate the origin of this extremely long decay time, we considered the density of disclination loops, as described below. We set the voltage at $\varepsilon=2.7$ above ε_t and monitored concomitantly the injected power and (optically) the DSM1$\rightarrow$DSM2 transition. After the DSM2 front has passed we abruptly switched off the driving voltage at different times t and immediately took a snapshot of optical image showing disclination loops. We found that P decreases monotonically in time in a similar fashion as shown in Figs. 8 and 9. However, there appears to be no corresponding variation in the density of disclination loops with t elapsed after the DSM2 front has passed. Consequently, the extremely slow decrease in P detected at DSM1$\rightarrow$DSM2 turbulence transition for dielectric EHC appears to be unrelated to an ongoing generation of disclinations in the liquid crystal director.

The density of disclination loops ρ is directly related to the averaged intensity of the transmitted light $\langle I\rangle$ [27]. Therefore, we also measured $\langle I\rangle$ integrated over 6.2% of the whole area of sample C. A sharp decrease of $\langle I\rangle$ by about 20% is observed at the DSM1$\rightarrow$DSM2 transition (at $t=0$) within $t=60$ s (the time corresponding to the DSM2 front passing the viewing area) without any indication of a slow time decay as measured for the injected power as shown in the inset of Fig. 9. Therefore, the long-time decrease in P demonstrated in Figs. 8 and 9 remains still puzzling. It may involve interactions between the disclination loops [26] not detected by experimental methods presented here.

Another puzzle is that no apparent signature in the Nusselt number has been found for the DSM1$\rightarrow$DSM2 turbulence transition in conductive EHC [15]. Therefore, we have performed more focussed measurements of the injected power around this transition point. Figure 10 displays the time dependence of P for two different values of ε as indicated with the transition point being set at $t=0$. As one can see, the DSM1$\rightarrow$DSM2 turbulence transition in conductive EHC is characterized with a single peak in $P(t)$, a quite different behavior from that measured for dielectric DSM1$\rightarrow$DSM2 transition [an exponential decay of $P(t)$ with an extremely slow decay time as shown in Fig. 8]. Note that peaks in Fig. 10 represent an increase of only about 3% in P and that the time scale of the whole peak is not more than about 60 s (time approximately corresponding to the passing time of the DSM2 front through the whole sample). Taking into account these scales, it is understandable that the DSM1$\rightarrow$DSM2 turbulence transition in conductive EHC remained unnoticed in electric Nusselt-number measurements under experimental conditions reported in Ref. [15] [similar to those in Fig. 2(a)].

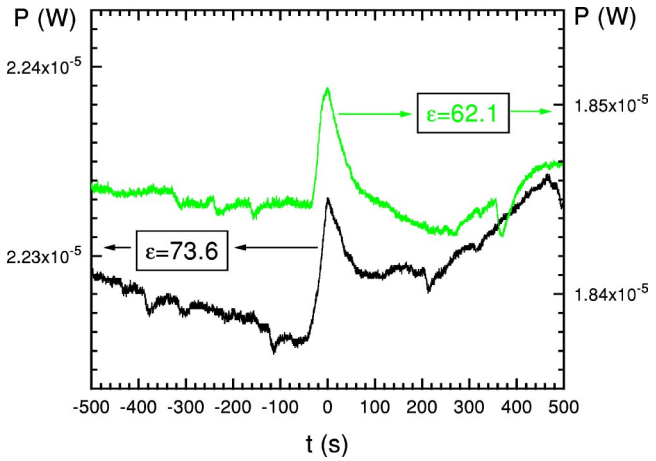

FIG. 10. (Color online) Electric power vs time near the DSM1 $\rightarrow$DSM2 turbulence transition (taking place around $t=0$) in conductive EHC ($T=50\,^{\circ}\mathrm{C}$) for two different ε as indicated in the figure.

Under different experimental conditions, however, we were able to obtain the response in the electric properties to the DSM1$\rightarrow$DSM2 transition in conductive EHC similar to that in dielectric EHC [Fig. 2(b)]. Figure 11 shows the voltage dependence of the conductivity of cell C at $T=50\,^{\circ}\mathrm{C}$ obtained from fluctuation measurements. The main difference between Figs. 11 and 2(a) (as well as Fig. 1 of Ref. [15]) is in the ramping rate r. Data in Fig. 11 have been obtained with $r\approx 0.25$ mV/s while those in Fig. 2(a) (as well as data reported in Ref. [15]) with r larger by about an order of magnitude. Note that both of these ramping rates are of the order of magnitude, at which the hysteresis of the DSM1$\rightarrow$DSM2 is expected to diminish [23,29]. Therefore, it still remains unclear why we do see the DSM1$\rightarrow$DSM2 transition in the form of a local minimum in $G(\varepsilon)$ [similar, but not so expressed as for dielectric EHC—Fig. 2(b)] at extremely low r and we do not see at somewhat higher r [15].

The inset of Fig. 11 shows the blowup of $G(\varepsilon)$ at the low voltage range. It is useful to compare this graph with the

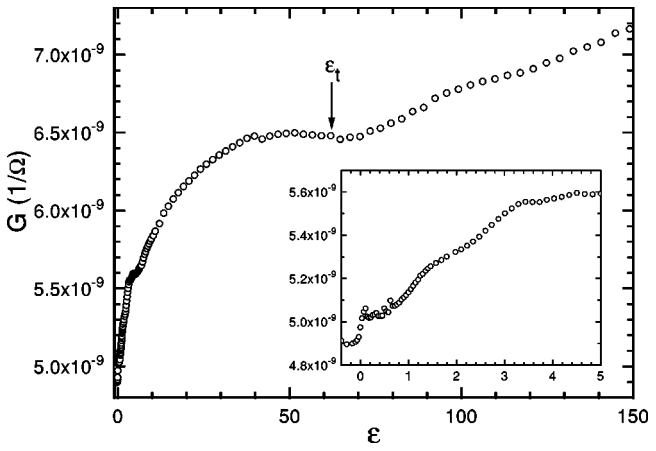

FIG. 11. Voltage dependence of the conductivity G in conductive EHC ($T=50\,^{\circ}\mathrm{C}, f=100$ Hz) obtained from long-time fluctuation measurements. Inset: blowup of the low voltage region.

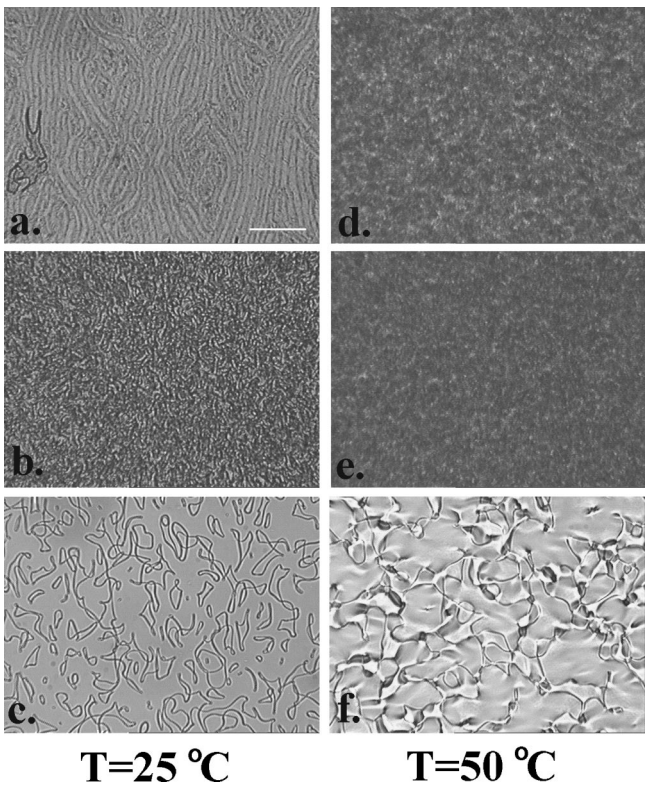

FIG. 12. Snapshots of DSM1 [(a) and (d)], DSM2 [(b) and (e)] patterns as well as the images of the disclination loops taken immediately after switching off the driving voltage. (a)–(c) dielectric EHC ($T=25\,^{\circ}\mathrm{C}, \varepsilon=2.7$); (d)–(f) conductive EHC ($T=50\,^{\circ}\mathrm{C}, \varepsilon=62.1$). The scale bar in (a) shows 100 μm.

corresponding data (empty symbols) in Fig. 4 (recorded concomitantly), because all the voltage dependences correlate in these two graphs and several EHC transitions are captured. At EHC threshold $\varepsilon=0$, G increases sharply but no increase in $\sigma_P/\langle P\rangle$ has been detected. At the threshold of defect turbulence, $\varepsilon\approx 0.2$, $\sigma_P/\langle P\rangle$ increases sharply (Fig. 4), G, however, stops to increase (inset of Fig. 11). At $\varepsilon\approx 0.7$ (defect turbulence), $\sigma_P/\langle P\rangle$ reaches its maximum and G has a change in its slope. At $\varepsilon\approx 1.4$ (still defect turbulence), $\sigma_P/\langle P\rangle$ starts to decrease and G again has a slight change in its slope. At $\varepsilon\approx 3.3$ the increase of G slows down (Fig. 11) and at the same time, the decrease in $\sigma_P/\langle P\rangle$ also slows down. This presumably represents the route to the transition from defect turbulence to DSM1 where coherent oscillations in $g_a(t)$ diminish (at $\varepsilon\approx 5$).

Optical images recorded at the DSM1$\rightarrow$DSM2 transition also demonstrate substantial differences in the nature of this transition in the dielectric and in the conductive EHC. Figure 12 shows snapshots of DSM1 and DSM2 patterns as well as that of the relaxing disclination loops (recorded immediately after switching off the driving voltage) for both dielectric [Figs. 12(a–c)] and conductive EHC [Figs. 12(d–f)].

Dielectric DSM1 pattern [Fig. 12(a)] substantially differs from the conductive DSM1 one [Fig. 12(d)]: the former shows an expressed spatiotemporal order, while for the latter no such order can be found. On the other hand, DSM2 patterns in dielectric [Fig. 12(b)] and conductive [Fig. 12(e)] do

not differ significantly: none of them has spatiotemporal order, and the only difference we could detect between them is that the transmitted light intensity fluctuations are much faster in conductive EHC than in dielectric EHC [that is why Fig. 12(e) appears to be more blurred than Fig. 12(b)].

As a consequence of the above statements, the DSM1 $\rightarrow$DSM2 turbulence transition in dielectric EHC is different from that in conductive EHC not only regarding the injected power (compare Figs. 8 and 10) but also in optical properties. In dielectric EHC, the DSM1 [Fig. 12(a)] to DSM2 [Fig. 12(b)] transition appears as a transition from a state with spatiotemporal order to a state without such order. The transition itself is also characterized by a substantial change in transmitted light intensity averaged over a large area of the sample. On the contrary, DSM1 [Fig. 12(d)] to DSM2 [Fig. 12(e)] transition in conductive EHC does not involve a change in the spatiotemporal order nor a significant change in the transmitted light intensity (compared to that in dielectric EHC), which is in agreement with previous observations at voltages close to ε_t [29].

Figures 12(c) and 12(f) show the relaxation of disclination loops recorded immediately (within $t=0.44$ s) after switching off the driving voltage in dielectric and in conductive EHC, respectively. Two distinct differences can be seen between Figs. 12(c) and 12(f). The density of the disclination loops ρ is much larger for dielectric DSM2 [Fig. 12(c)] than that following the conductive DSM2 [Fig. 12(f)]. The cause of this difference in ρ is still unknown. ρ depends on the applied voltage ε [24], however, transitions presented in Fig. 12 are quite close to the DSM1$\rightarrow$DSM2 transition ($\varepsilon_2 < 0.4$ using the nomenclature presented in Fig. 7 of Ref. [24]) and consequently, no large difference in ρ should be expected. The relaxation of the EHC pattern is much slower for conductive EHC than that for dielectric EHC. Figure 12(f) shows that the conductive EHC pattern is not relaxed completely at $t \approx 0.44$ s after switching off the driving voltage, while at the same time for dielectric EHC the relaxation is already finished. This behavior is easy to understand taking into account that the restoring forces towards quiescent state depend on the Frank elastic constants. Previous measurements on M5 have shown that the elastic constants are smaller by about a factor of 2 at $T=50\,^{\circ}\mathrm{C}$ than those at $T=25\,^{\circ}\mathrm{C}$ [40]. Consequently, the restoring forces present in Fig. 12(c) are much larger than those present in Fig. 12(f).

IV. DISCUSSION AND CONCLUSION

Extensive experimental studies have been performed regarding the conductivity and the fluctuations of injected electric power in electroconvection of a nematic liquid crystal, focusing on defect turbulence, anisotropic turbulence (DSM1), and on isotropic turbulence (DSM2).

The voltage dependence of the conductivities clearly shows an increased energy dissipation at the EHC threshold $\varepsilon=0$ both for conductive and dielectric convection. Above $\varepsilon=0$, conductivity measurements show a crossover in G between the data recorded with increased voltage steps and those measured with decreased voltage steps. For dielectric EHC this crossover occurs just above the threshold ε_t and could be caused by the pronounced hysteretic behavior of this transition [see Figs. 3(c) and 3(d)]. For conductive EHC the crossover shown in Fig. 2(a) is presumably caused by defect turbulence to anisotropic turbulence transition (where low-frequency, persistent oscillations diminish from the autocorrelation function of the fluctuations).

The apparent decrease of G above ε_t in dielectric EHC with the increase of ε [inset of Fig. 2(b)] in terms of the electric Nusselt number $\mathcal{N}$ [15] means a decrease of $\mathcal{N}$ with the increase of the driving force. Such a behavior, already observed in conductive EHC (however, at much larger ε [15]) to the best of our knowledge has not been detected in other turbulent systems and therefore, it represents a challenge for more detailed studies. The DSM1$\rightarrow$DSM2 transition in dielectric EHC has another signature in the electric properties: the decrease in the width of the fluctuations (see the inset of Fig. 8) is larger than the decrease in absolute value of P (see the main plot in Fig. 8) which causes a small, but sharp decrease of $\sigma_P/\langle P\rangle$ at ε_t (see Fig. 4).

The most remarkable differences between the conductive and dielectric regimes are found in the defect turbulence states. As already described in Ref. [21] the conductive convection in the defect turbulence voltage range $\varepsilon_d \leqslant \varepsilon \leqslant \varepsilon_t$ is characterized with a dramatic increase of $\sigma_P/\langle P\rangle$ above ε_d (Fig. 2, empty symbols), with low-frequency quasiperiodic fluctuations in $P-\langle P\rangle$ [Fig. 5(a), black line] that cause a persistent, slow oscillations in $g_a(t)$ [Fig. 6(a)] and with a Gaussian PDF (Fig. 7, filled symbols). The source of these characteristics lays in the dynamic process of creation/annihilation of conductive defects [21]. On the contrary, in dielectric EHC no significant increase of $\sigma_P/\langle P\rangle$ has been observed above ε_d nor a detectable difference in the spectra of fluctuations [Fig. 5(b)]. Consequently, as one could expect, the persistent, low-frequency oscillations in $g_a(t)$ are also absent in dielectric EHC [Fig. 6(b)] despite the rather ordered spatial distribution of the defects [see, e.g., Fig. 3(d)]. Moreover, for dielectric EHC the PDFs in the voltage range of $\varepsilon_d \leqslant \varepsilon \leqslant \varepsilon_t$ obey a non-Gaussian distribution (Fig. 7, empty symbols). Similar, non-Gaussian statistics have been found in various other systems with convecting fluids experimentally such as in Rayleigh-Bénard convection [13], turbulent swirling flow in closed geometry [1,9,10], or in fluctuations of the Danube water level [3] as well as mathematically [2,11]. All of these fluctuations obey the same, universal non-Gaussian statistics: the high (positive) end of PDF is close to Gaussian, the maximum of the distribution is slightly shifted towards positive values, while the low (negative) end of PDF has a distinct exponential tail. According to Refs. [1,10] the existence of the exponential tail is due to events of fluid motion (with a large-scale extension both in space and time) spanning the entire closed system. This explanation is supported by measurements on turbulent swirling flow in open geometry [9], in which no exponential tail has been found and the fluctuations became Gaussian. However, the PDF shown in Fig. 7 for EHC in the dielectric regime (open symbols), exhibits all the above-mentioned characteristics of non-Gaussian statistics, except the low (negative) end of the distribution decays slower than an ex-

ponential, but still not Gaussian. The details of this are under investigation.

In summary, distinct differences in the electric properties between conductive and dielectric EHC have been found regarding (i) the normalized standard deviation, (ii) the spectra, and (iii) the probability density distribution of the electric power fluctuations in the defect turbulence voltage range. A robust electric response of the anisotropic-isotropic turbulent transition has been also captured in dielectric EHC. On the contrary, in the convective EHC ε_t has much less distinct signature in the electric properties in accordance with the results of Ref. [15]. The cause of this difference is still unclear. One possible explanation is the observation that the increase of the density of disclination loops ρ is much larger at dielectric DSM1→DSM2 [Fig. 12(c)] than at conductive DSM1→DSM2 [Fig. 12(f)]. If one consider DSM1→DSM2 transition as a ''transition from a structured two-dimensional (2D) turbulence towards a structureless 3D turbulence'' [28], the decrease of P at ε_t observed in dielectric EHC becomes understandable, since such a transition must involve an increase in the number of degrees of freedom excited. However, in this framework the absence of decrease of P at DSM1→DSM2 transition in conductive EHC still remains unexplained.

ACKNOWLEDGMENTS

We have benefitted from discussions with W. Goldburg. The work was supported by the National Science Foundation under Grant No. DMR-9988614.

[1] S.T. Bramwell, P.C.W. Holdsworth, and J.-F. Pinton, Nature (London) **396**, 552 (1998).
[2] S.T. Bramwell, K. Christensen, J.-Y. Fortin, P.C.W. Holdsworth, H.J. Jensen, S. Lise, J. López, M. Nicodemi, J.-F. Pinton and M. Sellitto, Phys. Rev. Lett. **84**, 3744 (2000).
[3] S.T. Bramwell, T. Fennel, P.C.W. Holdsworth, and B. Portelli, Europhys. Lett. **57**, 310 (2002).
[4] S. Ashkenazi and V. Steinberg, Phys. Rev. Lett. **83**, 4760 (1999); **83**, 3641 (1999).
[5] E. Villermaux, Phys. Rev. Lett. **75**, 4618 (1995).
[6] X.-L. Qiu, S.H. Yao, and P. Tong, Phys. Rev. E **61**, R6075 (2000).
[7] X.-L. Qiu and P. Tong, Phys. Rev. Lett. **87**, 094501 (2001).
[8] X.-L. Qiu and P. Tong, Phys. Rev. E **66**, 026308 (2002).
[9] R. Labbé, J.-F. Pinton, and S. Fauve, J. Phys. II **6**, 1099 (1996).
[10] J.-F. Pinton, P.C.W. Holdsworth, and R. Labbé, Phys. Rev. E **60**, R2452 (1999).
[11] S. Aumaitre, S. Fauve, S. McNamara, and P. Poggi, Eur. Phys. J. B **19**, 449 (2001).
[12] B. Portelli, P.C.W. Holdsworth, and J.-F. Pinton, Phys. Rev. Lett. **90**, 104501 (2003).
[13] X.-L. Qiu and P. Tong, Phys. Rev. E **64**, 036304 (2001).
[14] T. Kai, S. Kai, and K. Hirakawa, J. Phys. Soc. Jpn. **43**, 717 (1977).
[15] J.T. Gleeson, Phys. Rev. E **63**, 026306 (2001).
[16] *Pattern Formation in Liquid Crystals*, edited by Á. Buka, and L. Kramer (Springer, New York, 1996).
[17] P. G. de Gennes and J. Prost, *The Physics of Liquid Crystals* (Clarendon Press, Oxford, 1993).
[18] S. Kai and K. Hirakawa, Prog. Theor. Phys. Suppl. **64**, 212 (1978).
[19] P. Coullet, L. Gil, and J. Lega, Phys. Rev. Lett. **62**, 1619 (1989); S. Kai and W. Zimmermann, Prog. Theor. Phys. Suppl. **99**, 458 (1989); G. Goren, I. Procaccia, S. Rasenat, and V. Steinberg, Phys. Rev. Lett. **63**, 1237 (1989); S. Nasuno, S. Takeuchi, and Y. Sawada, Phys. Rev. A **40**, 3457 (1989); S. Kai, N. Chizumi, and M. Kohno, *ibid.* **40**, 6554 (1989); S. Rasenat, V. Steinberg, and I. Rehberg, *ibid.* **42**, 5998 (1990); S. Rasenat, E. Braun, and V. Steinberg, *ibid.* **43**, 5728 (1991).
[20] S. Nasuno, O. Sasaki, S. Kai, and W. Zimmermann, Phys. Rev. A **46**, 4954 (1992).
[21] T. Tóth-Katona, J. R. Cressman, W. I. Goldburg, and J. T. Gleeson, Phys. Rev. E **68**, 030101(R) (2003).
[22] M. Scheuring, L. Kramer, and J. Peinke, Phys. Rev. E **58**, 2018 (1998).
[23] S. Kai, W. Zimmermann, M. Andoh, and N. Chizumi, Phys. Rev. Lett. **64**, 1111 (1990).
[24] S. Kai, W. Zimmermann, and M. Andoh, Mod. Phys. Lett. B **4**, 767 (1990).
[25] S. Kai, M. Andoh, and S. Yamaguchi, Phys. Rev. A **46**, R7375 (1992).
[26] H.M. Shehadeh and J.P. McClymer, Phys. Rev. Lett. **79**, 4206 (1997).
[27] V. Carbone, N. Scaramuzza, and C. Versace, Physica A **106**, 314 (1997).
[28] G. Strangi, C. Versace, N. Scaramuzza, D.E. Lucchetta, V. Carbone, and R. Bartolino, Phys. Rev. E **59**, 5523 (1999).
[29] D.E. Lucchetta, N. Scaramuzza, G. Strangi, and C. Versace, Phys. Rev. E **60**, 610 (1999).
[30] V.S.U. Fazio and L. Komitov, Europhys. Lett. **46**, 38 (1999).
[31] V.S.U. Fazio, F. Nannelli, and L. Komitov, Phys. Rev. E **63**, 061712 (2001).
[32] W.I. Goldburg, Y.Y. Goldshmidt, and H. Kellay, Phys. Rev. Lett. **87**, 245502 (2001).
[33] J. Shi, C. Wang, V. Surendranath, K. Kang, and J.T. Gleeson, Liq. Cryst. **29**, 877 (2002).
[34] J.T. Gleeson, N. Gheorghiu, and E. Plaut, Eur. Phys. J. B **26**, 515 (2002).
[35] S. Natuno, O. Sasaki, S. Kai, and W. Zimmermann, Phys. Rev. A **46**, 4954 (1992).
[36] J.-H. Huh, Y. Yusuf, Y. Hidaka, and S. Kai, Phys. Rev. E **66**, 031705 (2002).
[37] J.-H. Huh, Y. Hidaka, Y. Yusuf, N. Éber, T. Tóth-Katona, Á. Buka, and S. Kai, Mol. Cryst. Liq. Cryst. **364**, 111 (2001).
[38] S. Kai and W. Zimmermann, Prog. Theor. Phys. Suppl. **99**, 458 (1989).
[39] T. Tóth-Katona and J. T. Gleeson, Phys. Rev. Lett. (to be published).
[40] R. Stannarius (private communication).